Available online at www.sciencedirect.com
ScienceDirect
Trans. Nonferrous Met. Soc. China 31(2021) 925−938
Transactions of Nonferrous Metals Society of China
www.tnmsc.cn

Microstructure and mechanical properties of as-cast and solid solution treated Mg−8Li−*x*Al−*y*Zn alloys

Xin-li LIANG[1], Xiang PENG[1], Hao JI[1], Wen-cai LIU[1], Guo-hua WU[1,2], Wen-jiang DING[1,2]

1. National Engineering Research Center of Light Alloy Net Forming, School of Materials Science and Engineering, Shanghai Jiao Tong University, Shanghai 200240, China;
2. State Key Laboratory of Metal Matrix Composite, School of Materials Science and Engineering, Shanghai Jiao Tong University, Shanghai 200240, China

Received 19 May 2020; accepted 24 December 2020

Abstract: The effects of Al/Zn ratio (mass ratio) on microstructure and mechanical properties of the Mg−8Li alloy were investigated. The results indicate that in the as-cast Mg−8Li−*x*Al−*y*Zn (*x*+*y*=5) alloys (LAZ alloys), when the Al/Zn ratio is 1:4 and 2:3, the secondary phases are mainly AlLi and MgLiZn phases; when the Al/Zn ratio is 3:2 and 4:1, the secondary phases are mainly AlLi and $MgLi_2Al$ phases. The decomposition temperature of MgLiZn phase is about 300 °C and the decomposition temperatures of AlLi phase and $MgLi_2Al$ phase are higher (~350 °C). Solid solution strengthening is the main factor for the improvement of strength of Mg−8Li−*x*Al−*y*Zn alloys. The Mg−8Li−3Al−2Zn alloy after solution treatment at 350 °C for 4 h has the best comprehensive mechanical properties (yield strength of 272.5 MPa, ultimate tensile strength of 315.0 MPa and elongation of 3.4%) among the studied as-cast and solid solution treated Mg−8Li−*x*Al−*y*Zn alloys.

Key words: Mg−Li alloy; Al/Zn ratio; microstructure; mechanical properties

1 Introduction

Mg−Li alloys are the lightest metal engineering materials, which have been widely applied in aerospace, military and electronics because of their low density (1.30−1.65 g/cm^3), high specific strength and stiffness [1−3]. Besides, Mg−Li alloys also have promising prospects in future industrial applications due to their excellent electromagnetic shielding properties, damping capacity and machinability [4]. According to the Mg−Li equilibrium phase diagram, when Li content is between 5.3 wt.% and 10.7 wt.%, the Mg−Li alloy is composed of α-Mg (hcp) and β-Li (bcc) phases. The dual-phase Mg−Li alloy combines the strength of α-Mg with the plasticity of β-Li, which ensures the alloy to own good ductility and formability compared to magnesium alloy. However, the disadvantage of low strength limits its further application to some extent.

A lot of researches have been conducted to overcome the shortcomings of Mg−Li alloys by adding alloying elements. Among them, Al and Zn elements are the two most effective alloying elements to strengthen the Mg−Li alloys. Many Mg−Li alloys with the third elements have been prepared and studied, such as Mg−Li−Al, Mg−Li−Zn and Mg−Li−Al−Zn alloys [5−8]. Different contents of Al and Zn have different effects on Mg−Li alloys. Al element strengthens the Mg−Li alloys mainly through solid solution strengthening and precipitation strengthening, wherein the strengthening phase $MgLi_2Al$ is a metastable phase

Corresponding author: Wen-cai LIU, Tel: +86-21-54742630, Fax: +86-21-34202794, E-mail: liuwc@sjtu.edu.cn; Guo-hua WU, E-mail: ghwu@sjtu.edu.cn
DOI: 10.1016/S1003-6326(21)65550-4

and decomposes into an equilibrium phase AlLi during high temperature or room temperature aging to soften the alloy [9−11]. Zn element mainly plays a solid solution strengthening effect in the Mg−Li alloy, and intermediate compounds such as Mg_7Zn_3 are present in Mg−Li−Zn alloy when zinc content is high [12−14]. However, Al and Zn should not be excessive, otherwise the precipitates will be coarse to deteriorate mechanical properties [12]. Heat treatment is an effective way to strengthen Mg−Li alloys, and some researches have also been carried out [15−17]. However, the effect of Al/Zn ratio on microstructure and properties of dual-phase Mg−Li alloy has rarely been reported.

Based on the previous researches, the Mg−8Li alloy was selected as the base alloy, and the total content of Al and Zn elements was 5 wt.% to obtain good comprehensive performance. The microstructure and mechanical properties of Mg−8Li−*x*Al−*y*Zn (*x*=1, 2, 3, 4; *y*=4, 3, 2, 1) alloys with different Al/Zn mass ratios (*x*:*y*=1:4; 2:3; 3:2 and 4:1) were investigated, and the optimal ratio was obtained in this study. In addition, the effects of solid solution treatment on microstructure and mechanical properties of Mg−Li alloy with different Al/Zn ratios were studied.

2 Experimental

In this study, commercially pure Mg, Li, Al and Zn were used to prepare Mg−8Li−*x*Al−*y*Zn alloys (LAZ alloys). These raw materials were melted in a vacuum induction furnace under the protection of argon at 3×10^4 Pa. Mechanical stirring was carried out at 650 °C for 3 min in order to make the melt homogeneous. The melt was held for seven minutes when the temperature rose to 700 °C, then poured into a preheated steel mold. Some as-cast specimens were solid solution treated at 300 and 350 °C for 4 h, respectively. All the samples were taken from the bottom of the ingot and prepared into dog-bone tensile specimens with gauge sizes of 15 mm × 3 mm × 2 mm for tensile test.

The chemical compositions of the studied alloys were determined by inductively coupled plasma–atomic emission spectrometry (ICP−AES) and listed in Table 1. These studied alloys were named LAZ814, LAZ823, LAZ832 and LAZ841 according to different Al and Zn contents. The microstructure was analyzed by optical microscope (OM; ZEISS) and scanning electron microscope (SEM; Phenom XL) equipped with an energy dispersive spectroscope (EDS). The phase analysis was characterized by an X-ray diffractometer (XRD; Ultima IV) with a resource of Cu K_α radiation at a scan rate of 5 (°)/min and a step size of 0.02°. Transmission electron microscope (TEM, JOEL 2100, 200 kV) was used to observe the size and morphology of the precipitates. The specimens for TEM observation were mechanically thinned to ~60 μm and then polished by argon ion milling (Gatan 691). Tensile properties of the studied alloys at room temperature were tested on the tensile machine (Zwick/Roell) at a cross-head speed of 1 mm/min, and the fracture surface was analyzed by SEM.

Table 1 Chemical compositions of studied alloys (wt.%)

Alloy	Li	Al	Zn	Mg
LAZ814	8.25	1.16	4.01	Bal.
LAZ823	8.30	2.25	3.11	Bal.
LAZ832	7.97	3.29	1.81	Bal.
LAZ841	8.02	4.36	0.95	Bal.

3 Results

3.1 Microstructures

The optical microstructures of the as-cast LAZ alloys are shown in Fig. 1, indicating that the as-cast LAZ alloys are primarily composed of *α*-Mg, *β*-Li and some precipitates mainly distributed in *β*-Li. *α*-Mg is basically blocky and stripe-like with sharp edges and different sizes. Meanwhile, it is worth noting that the amount of precipitates is also significantly reduced as the Zn content decreases. Figure 2 shows the XRD patterns of the as-cast specimens. *α*-Mg and *β*-Li are the major phases in the LAZ alloys according to the XRD result. It is worth noting that when the Al/Zn ratio 1:4 and 2:3, the secondary phases in the LAZ814 and LAZ823 alloys are mainly AlLi and MgLiZn [12], but when the Al/Zn ratio is 3:2 and 4:1, the secondary phases in the LAZ832 and LAZ841 alloys are mainly AlLi phase and $MgLi_2Al$ phase. From the result of XRD, the peak intensity of AlLi in the LAZ alloy increases with the increase of Al content, and the new peaks (at 2θ values of 22° and 45°) appearing in LAZ814 and LAZ823 are MgLiZn phase.

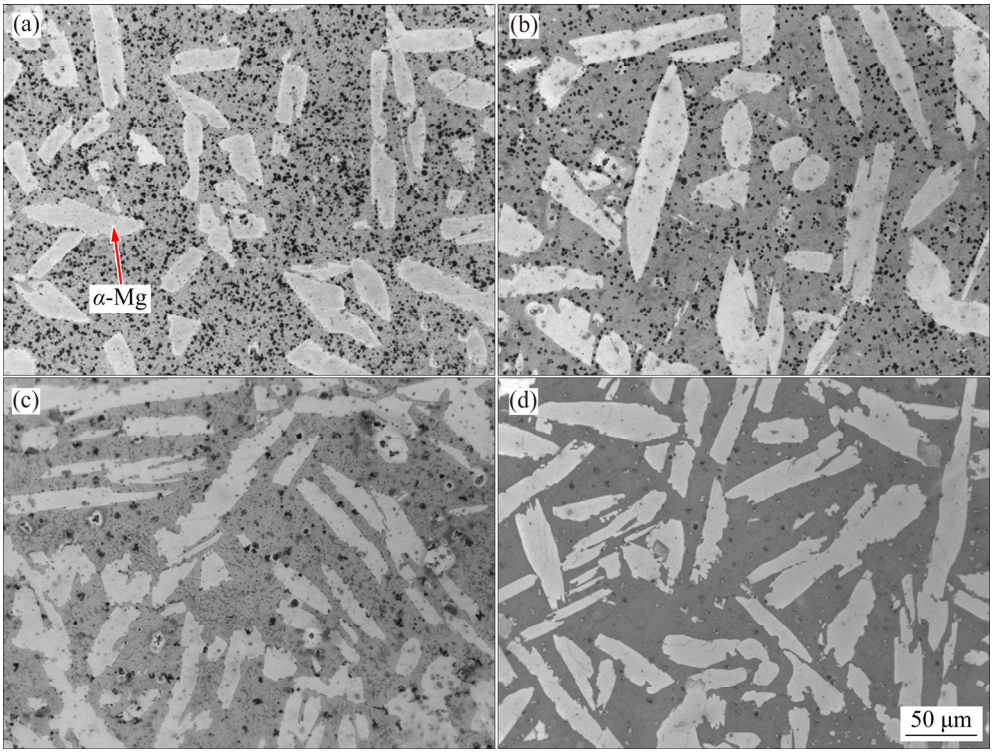

Fig. 1 Optical micrographs of as-cast LAZ alloys: (a) LAZ814; (b) LAZ823; (c) LAZ832; (d) LAZ841

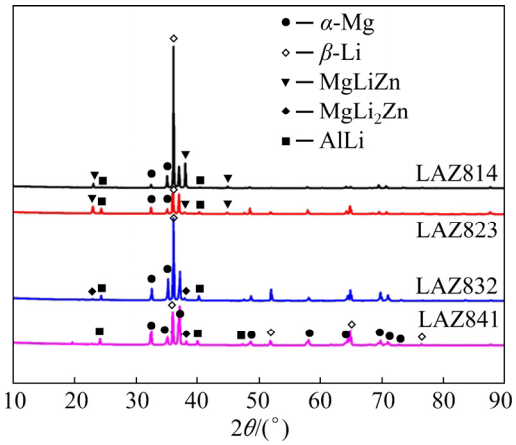

Fig. 2 XRD patterns of as-cast LAZ alloys with different Al/Zn ratios

In order to investigate the distribution of secondary phases in LAZ alloys, SEM analysis was conducted. Figure 3 shows high resolution SEM images and EDS analysis results of the secondary phases in the as-cast LAZ alloys. It can be seen from the results that the particles in the LAZ alloys mainly include visible micron-sized particles and some nano-scale ultra-fine particles that are difficult to see. In the SEM images (Figs. 3(a−d)), as the Al content increases and the Zn content decreases, the secondary particles gradually decrease, which is consistent with the optical microstructure result. According to the XRD results, it can be inferred that these large-sized visible particles are MgLiZn phase [18] and tiny large-sized AlLi or $MgLi_2Al$ particles. The diffraction intensity of AlLi phase increases as the Al content increases in these four LAZ alloys, which cannot be found in the OM and SEM images. Besides, the MgLiZn phases are mainly distributed along the α-Mg grain boundaries and some other particles are located inside the β-Li matrix [14,19]. When the Al/Zn ratio is 3:2 and 4:1, there are elongated irregular precipitates along the α-Mg grain boundaries, and the shape of the precipitates distributed in the β-Li matrix is irregular.

EDS point scanning and mapping scanning were performed to further determine the chemical formula of the precipitates and the distribution of elements. The EDS point scanning results are listed in Table 2. It can be seen in Fig. 3(a) that, in LAZ814 alloy, some of the precipitates (labeled as B) are composed of Mg and Zn elements. It should be noted that the EDS device cannot detect the presence of Li element because the spectrum is cut off for all elements below boron, but combined with the XRD result it can be judged that the secondary particle is MgLiZn [13]. Some precipitates (labeled as C) in Fig. 3(b) contain Mg, Al and Zn elements.

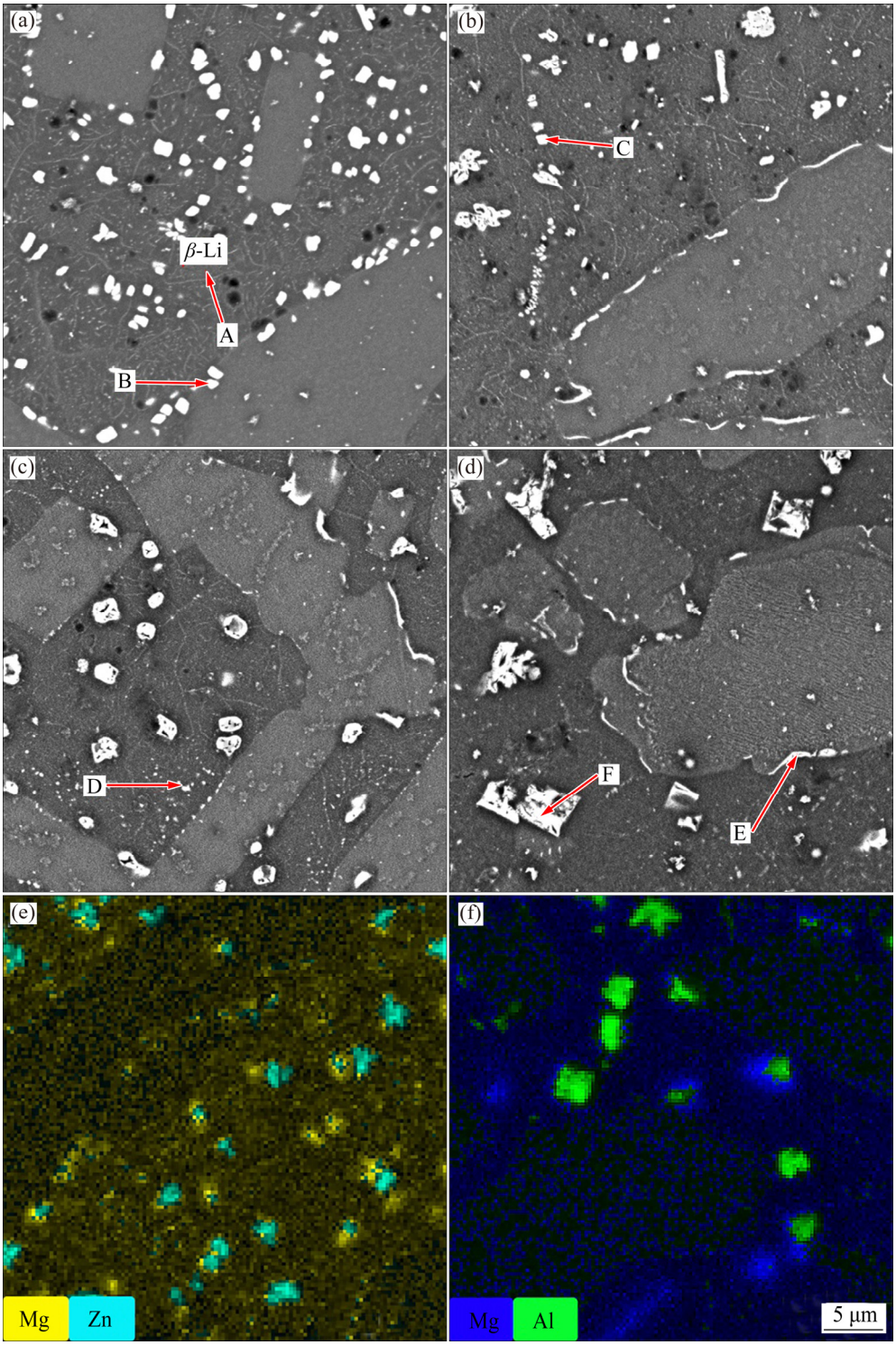

Fig. 3 High resolution SEM images (a−d) and EDS mapping scanning (e, f) of as-cast alloys of LAZ814 (a), LAZ823 (b), LAZ832 (c) and LAZ841 (d), and EDS mapping scanning of LAZ814 (e) and LAZ841 (f)

Considering the fact that Zn element will be dissolved into the matrix, it can be thought that tiny amount of Zn element detected is derived from the matrix, and combined with XRD results, it can be judged that these secondary particles are AlLi phase. In Figs. 3(c, d), some precipitates contain Mg and Al elements, and some contain Mg, Al and Zn elements. According to the previous experiment [14], the precipitates in the LAZ832 and LAZ841 alloys are AlLi (labeled as D) and $MgLi_2Al$ (labeled as E and F). The slender $MgLi_2Al$ phase instead of MgLiZn phase is mainly

Table 2 EDS point scanning results of four as-cast LAZ alloys

Location in Fig. 3	Content/at.%		
	Mg	Al	Zn
A	98.7	0.3	1.0
B	95.5	−	4.5
C	85.9	12.5	1.6
D	82.9	15.7	1.4
E	76.9	20.5	2.6
F	88.9	9.8	1.3

distributed along the α-Mg grain boundaries in the LAZ832 and LAZ841 alloys. The secondary particles distributed in the β-Li matrix coarsen gradually as the Al content increases. The EDS mapping scanning image in Fig. 3(e) shows the distribution of Mg and Zn elements in the LAZ814 alloy. Zn is present in both the matrix and the secondary phase. Figure 3(f) shows the distribution of Mg and Al elements in the LAZ841 alloy, indicating that Al element is mainly distributed in the precipitates.

Figure 4 shows high resolution TEM micrographs of the as-cast LAZ814 and LAZ841 alloys, in which α-Mg and β-Li phases were detected. TEM analysis was applied to further identifying the secondary phase in the LAZ841 alloy. As shown in Figs. 4(c, d), the SAED pattern of the LAZ841 alloy indicated that the round and rod-shaped secondary phases are of FCC structure, which can be AlLi and $MgLi_2Al$ phases [20,21] because both AlLi and $MgLi_2Al$ phases have FCC structures and similar lattice parameters [22] as listed in Table 3. The SAED results demonstrate that the AlLi precipitates can coexist with the ternary $MgLi_2Al$ phase. Consequently, Al−Li phase can be used as the general term for AlLi phase and $MgLi_2Al$ phase in some places in this work.

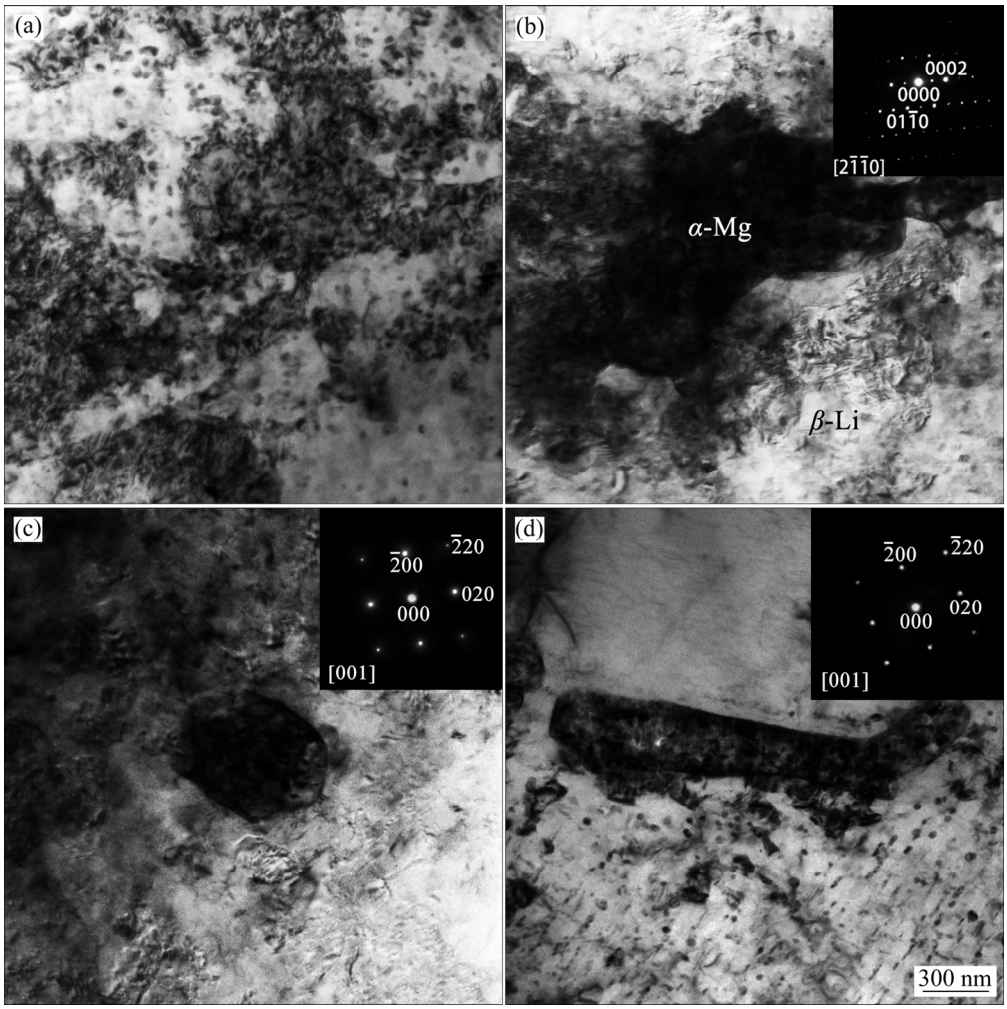

Fig. 4 High resolution TEM micrographs of as-cast LAZ814 (a), LAZ841 (b) and TEM micrographs of secondary phases showing round (c) and rod-shaped (d) Al−Li phase in LAZ841 alloy

Table 3 Lattice parameters and density of AlLi and $MgLi_2Al$

Phase	Lattice parameter				Density/ ($g \cdot cm^{-3}$)
	a/nm	*b*/nm	*c*/nm	*c*/*a*	
AlLi	0.638	0.638	0.638	1	1.735
$MgLi_2Al$	0.670	0.670	0.670	1	1.439

The SEM images and XRD patterns of the LAZ alloys after solid solution treatment at 300 °C for 4 h are shown in Figs. 5 and 6, respectively. The results show that the amount of precipitates in the LAZ814 and LAZ823 alloys (Figs. 5(a, b)) is significantly reduced after solid solution treatment compared with the as-cast LAZ814 and LAZ823 alloys (Figs. 1(a, b)), while the amount of precipitates in the LAZ832 and LAZ841 alloys has no significant change before and after solid solution treatment. However, α-Mg grain boundary of all the LAZ alloys after solid solution is smoothened, and the α-Mg in the LAZ832 alloy after solid solution at 300 °C for 4 h becomes strip-like. It is worth noting from Fig. 6 that the peak of the MgLiZn phase almost disappears, while the Al−Li phases still exist. This indicates that the decomposition temperature of the MgLiZn phase is relatively low and decomposes at ~300 °C.

The SEM images and XRD patterns of the LAZ alloys after solid solution treatment at 350 °C for 4 h are shown in Figs. 7 and 8, respectively. As the solid solution temperature increases to 350 °C, the number of secondary particles decreases, and the α-Mg grain boundary is further smoothened. From Fig. 8, it can be seen that the peak of metastable $MgLi_2Al$ phase disappears, but the peak of stable AlLi phase still exists, which is consistent with the results of EDS point scanning.

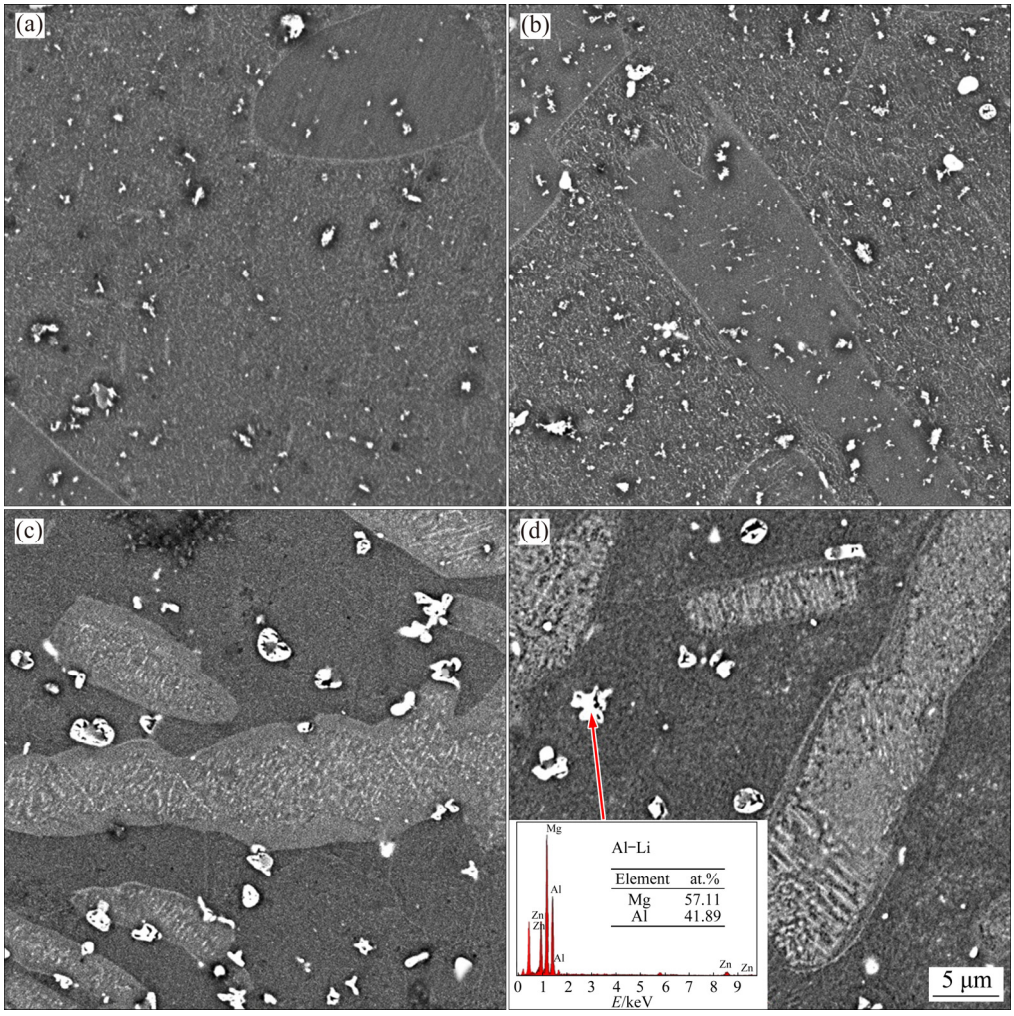

Fig. 5 SEM images of LAZ alloys after solid solution treatment at 300 °C for 4 h: (a) LAZ814; (b) LAZ823; (c) LAZ832; (d) LAZ841

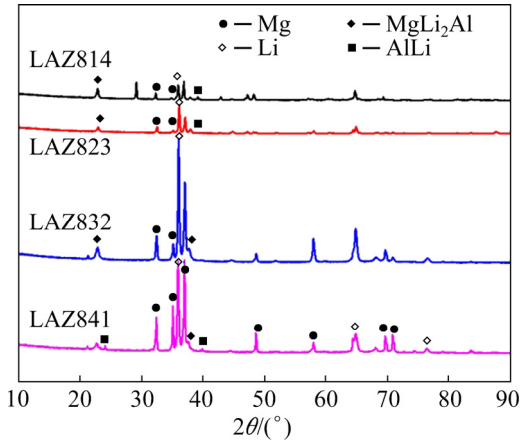

Fig. 6 XRD patterns of LAZ alloys after solid solution treatment at 300 °C for 4 h

3.2 Density and mechanical properties

Figure 9 shows the mechanical properties of the as-cast and solid solution treated LAZ alloys. According to Fig. 9(a), it is obvious that the ultimate tensile strength (UTS) of the as-cast alloys increases from 155.5 to 187.3 MPa as the Al/Zn ratio increases from 1:4 to 4:1, but the elongation (EL) decreases significantly from 45.3% to 10.0%. Figures 9(b, c) show the mechanical properties of the LAZ alloys after solid solution at 300 and 350 °C for 4 h, respectively. From the results, it is known that after the solution heat treatment at 300 °C for 4 h, the mechanical properties of the studied alloys are significantly improved. It is worth noting that with the increase of Al/Zn ratio, the strength increment of the four LAZ alloys decreases gradually. The tensile strength of the LAZ814 alloy increases most, from 155.5 MPa in the as-cast state to 271.9 MPa in the solid solution state. However, the plasticity of the studied alloys is reduced greatly. When the solid solution temperature increases from 300 to 350 °C, the YS (yield strength) and UTS of the LAZ814 alloy are basically unchanged, while the YS and UTS of the

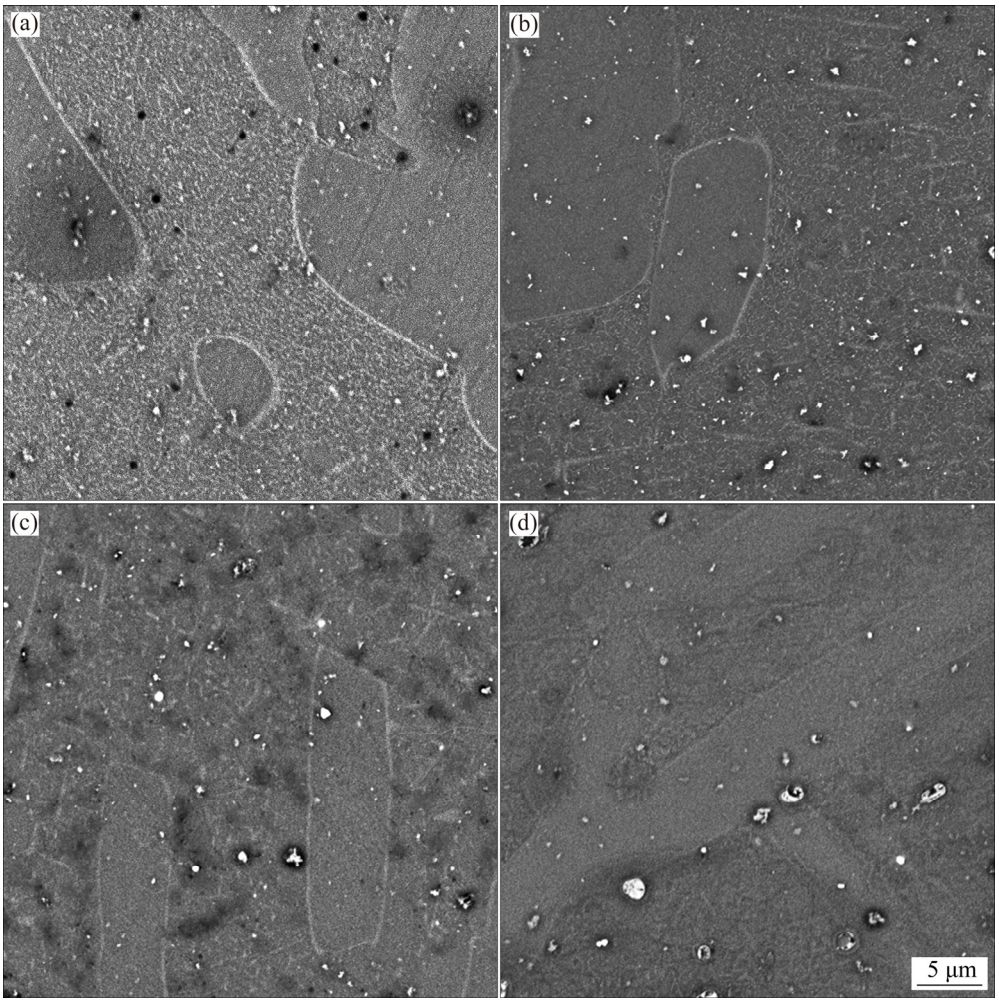

Fig. 7 SEM images of LAZ alloys after solid solution treatment at 350 °C for 4 h: (a) LAZ814; (b) LAZ823; (c) LAZ832; (d) LAZ841

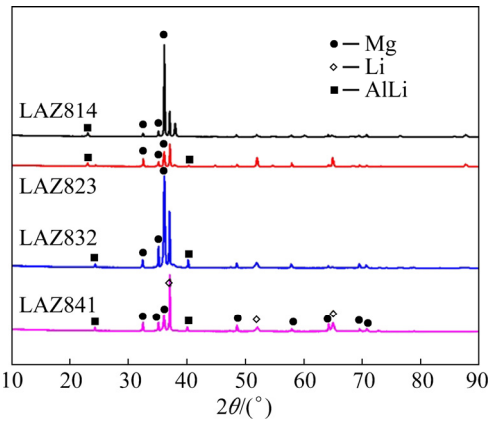

Fig. 8 XRD patterns of LAZ alloys after solid solution treatment at 350 °C for 4 h

LAZ823, LAZ832 and LAZ841 alloys are improved significantly, and the YS and UTS of the LAZ832 alloy increase from 193.5 and 248.5 MPa to 272.5 and 315.0 MPa, respectively. However, the EL of these alloys reduces a lot. The YS and UTS of the LAZ alloys after solid solution treatment are greater than those of most of other reported Mg−Li alloys.

3.3 Fracture behavior

Figure 10 shows the fracture surfaces of the as-cast LAZ alloys with various Al/Zn ratios. There are many dimples and tear ridges on the fracture surface. This is a typical plastic fracture in Mg−Li alloy [7,15]. In addition, the presence of secondary particles in the dimples indicates that the crack originates and propagates from the interface between the particles and the matrix. Through the XRD, SEM and EDS analysis mentioned above, it can be concluded that these particles in dimples are mainly AlLi, $MgLi_2Al$ and MgLiZn phases and they may be the fracture origin during the tensile testing. During the tensile process, on one hand, these secondary particles hinder the slip of dislocations. On the other hand, microcracks are generated around the secondary particles, and the expansion of the microcracks absorbs the strain energy. This is the strengthening mechanism of secondary particles. In addition, it is obvious that as Al/Zn ratio increases, the dimples become larger and shallower, indicating that the ductility of the alloy gradually decreases. This is consistent with the result of the plasticity of these LAZ alloys, which is gradually reduced as the Al/Zn ratio increases as shown in Fig. 9(a).

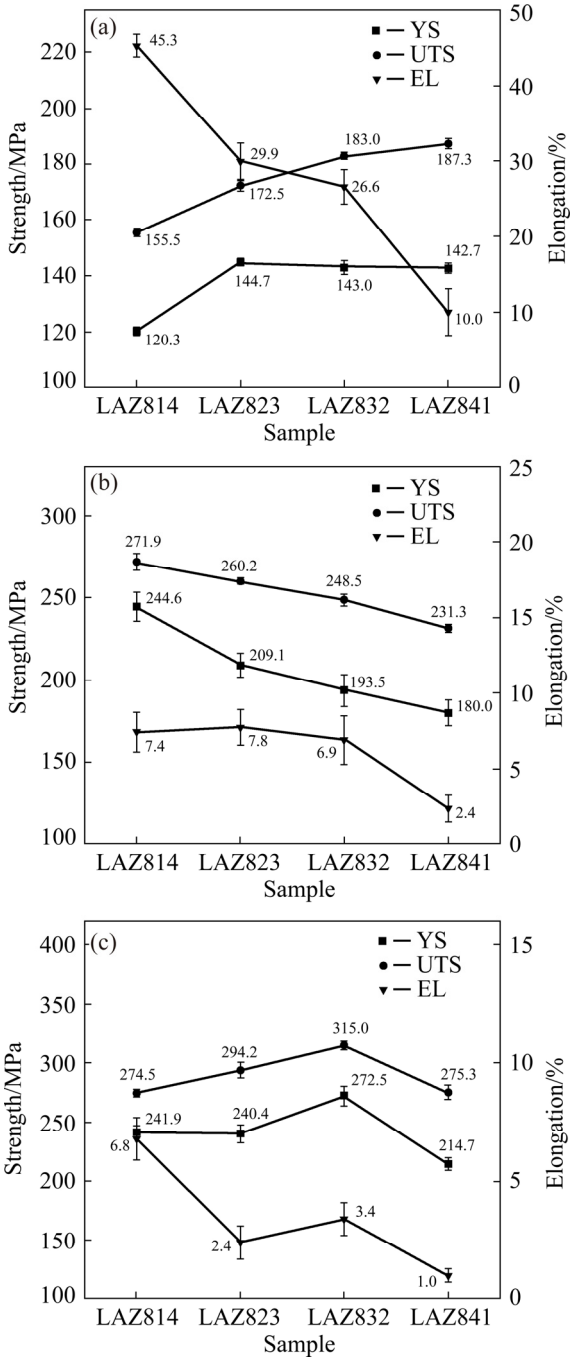

Fig. 9 Mechanical properties of LAZ alloys with different Al/Zn ratios: (a) As-cast LAZ alloys; (b) Solid solution treated LAZ alloys at 300 °C for 4 h; (c) Solid solution treated LAZ alloys at 350 °C for 4 h

Figure 11 shows the fracture surfaces of the solid solution treated LAZ alloy tensile samples. After the solid solution treatment at 300 °C for 4 h, the dimples on the fracture surface decrease obviously and several cleavage planes appear, indicating that the fracture mode of the studied alloys tends to quasi-cleavage fracture. And there are mixed characteristics of cleavage and ductile

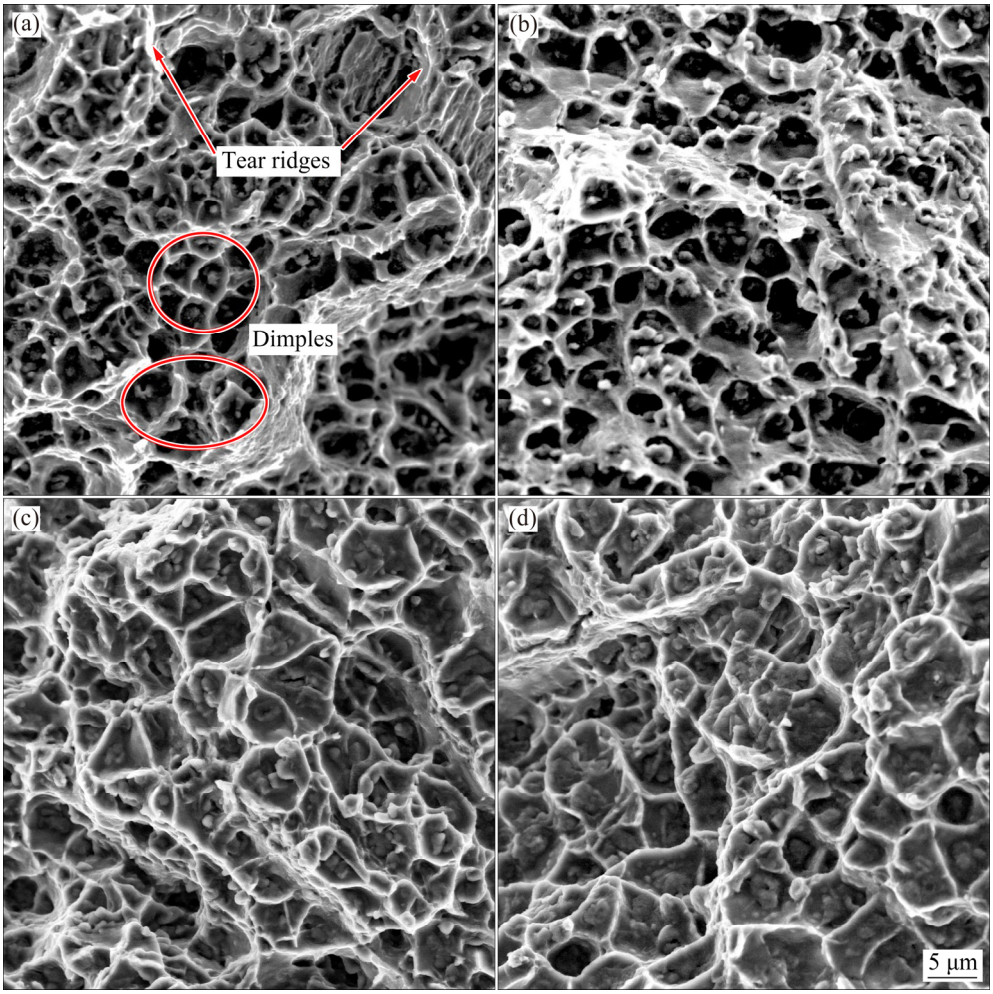

Fig. 10 Fracture surfaces of as-cast LAZ alloys with various Al/Zn ratios: (a) LAZ814; (b) LAZ823; (c) LAZ832; (d) LAZ841

fracture, which corresponds to a significant reduction in the elongation of the alloys shown in Fig. 9(b). After the solid solution treatment at 350 °C for 4 h, the fracture surfaces of these LAZ alloys transform into a typical cleavage fracture mode with river patterns. The fracture surface is primarily composed of cleavage planes and steps. Besides, the numbers of dimples and secondary particles decrease. This is related to the solid solution of the precipitates into the matrix.

4 Discussion

4.1 Effect of Al/Zn ratio on microstructure evolution

It has reported that the content variation of Al and Zn elements in the Mg−Li−Al−Zn alloy could influence the type and number of secondary particles in the casting process and the phase transition during heat treatment [20,23]. Different precipitates may occur in the Mg−Li alloys with different Al/Zn ratios. Al is added to the Mg−Li alloy mainly by forming AlLi and $MgLi_2Al$ phases acting as precipitation strengthening effect, while Zn is mainly solid-dissolved into the matrix when the content is low, which acts as solid solution strengthening. However, MgLiZn phase will emerge when the Zn content exceeds 2 wt.% [16,24]. Moreover, since the AlLi and $MgLi_2Al$ phases are invisible under the optical microscope due to their size, the number of the secondary particles in Fig. 1 decreases as the Zn content decreases. According to the results of the EDS point and mapping scanning in Fig. 3, Zn is mainly distributed in the secondary particles in the LAZ814 alloy and Al is mainly distributed in the secondary particles in the LAZ841 alloy. It can be concluded that, in the optical micrographs of the LAZ814 and LAZ823 alloys,

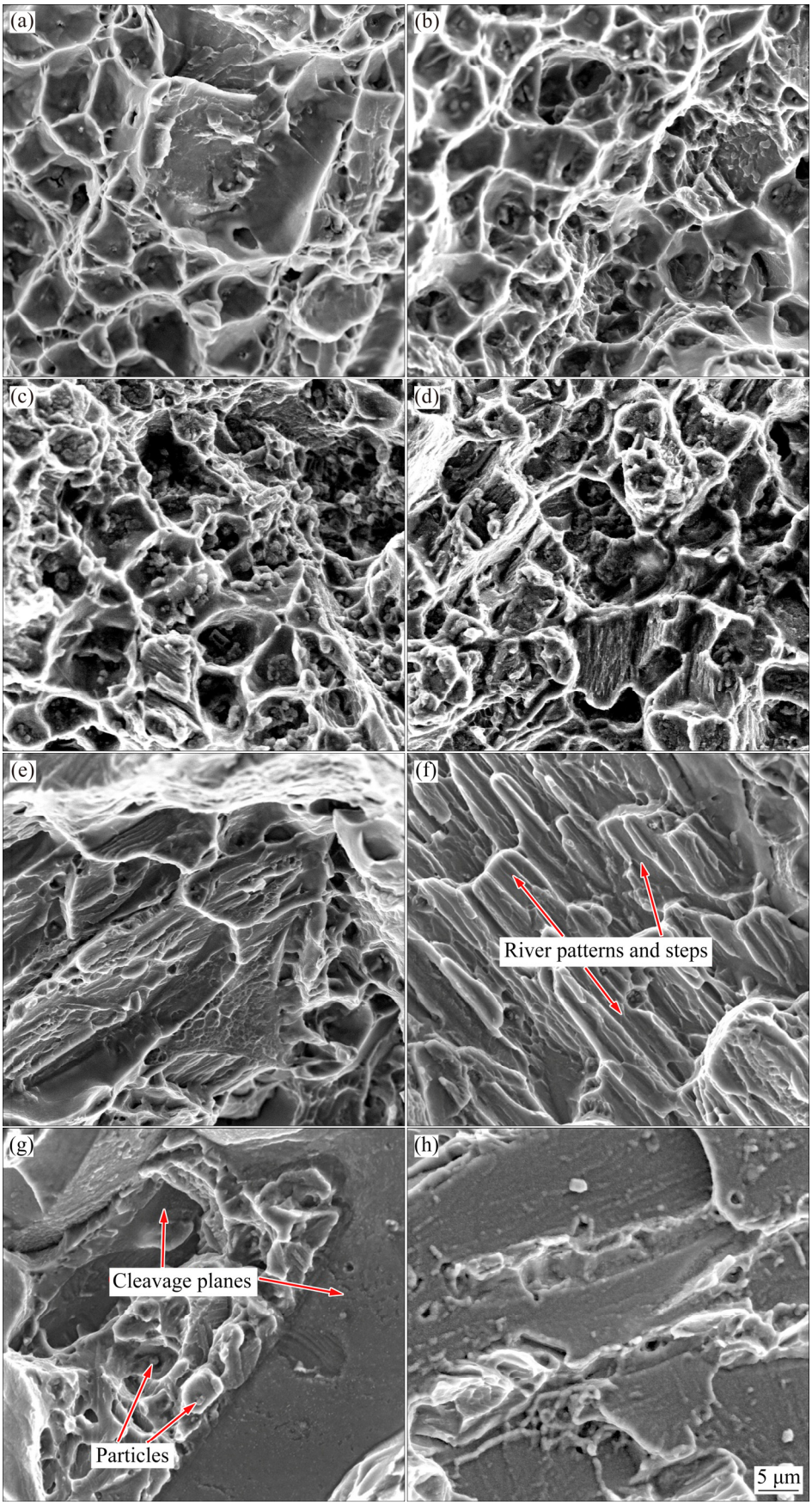

Fig. 11 Fracture surfaces of LAZ alloys after solid solution treatment at 300 °C for 4 h (a−d) and 350 °C for 4 h (e−h): (a, e) LAZ814; (b, f) LAZ823; (c, g) LAZ832; (d, h) LAZ841

those visible particles in the β-Li matrix are mainly MgLiZn phase, and the visible particles in the LAZ832 and LAZ841 alloys are mainly small amount of large-sized AlLi and $MgLi_2Al$ phases. Similar result has also been reported in the Mg−Li−Zn alloy. OROVCIK et al [12,13] pointed out that there are stable MgLiZn phase and metastable $MgLi_2Zn$ phase in the Mg−(6−8)Li−2Zn alloys and found their corresponding diffraction peaks. Figure 12 schematically illustrates the evolution of secondary particles in the LAZ alloys with different Al/Zn ratios. As the Al/Zn ratio increases, the MgLiZn phase gradually disappears, and only part of the visible large-sized Al−Li phases remain.

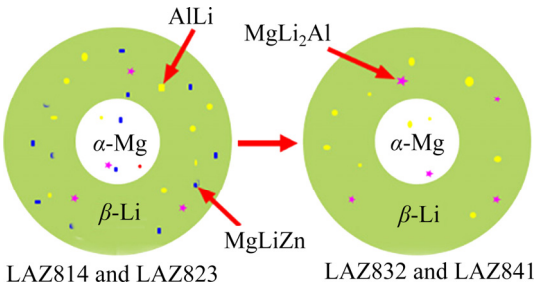

Fig. 12 Schematic diagram showing evolution of type and number of secondary phases in LAZ alloys with different Al/Zn ratios

It has been reported that AlLi phase in the Mg−Li alloy decomposes and dissolves into the matrix after solid solution treatment at a temperature exceeding 340 °C [20]. However, the MgLiZn phase will decompose when the temperature exceeds 300 °C or when it is overaged [13,25], which is in good accordance with this experiment. As for the micrographs shown in Fig. 5, after solid solution treatment at 300 °C for 4 h, the MgLiZn phase in the LAZ814 and LAZ823 alloys decreases significantly, and the metastable $MgLi_2Al$ phase decomposes at 300 °C, which is consistent with the previous report [15]. At the same time, the boundary of α-Mg also becomes smooth. The XRD patterns shown in Fig. 6 also demonstrate that the MgLiZn phase disappears after solid solution treatment at 300 °C for 4 h, and the remaining particles are mainly AlLi and $MgLi_2Al$ phases because of their higher decomposition temperatures [20].

After solid solution treatment at 350 °C for 4 h, the AlLi and $MgLi_2Al$ phases in LAZ alloys decompose, and the number of particles shown in the SEM images decreases. The results of EDS point scanning shown in Fig. 7 indicate that $MgLi_2Al$ particles decompose after solid solution treatment and only small amount of AlLi remains. In the XRD patterns shown in Fig. 8, the peaks of AlLi are found, but the peaks of MgLiZn and $MgLi_2Al$ phases disappear compared with the as-cast XRD patterns. Relevant research [26] suggests that when the Zn content in the Mg−Li alloy is less than 4%, Zn mainly dissolves into the matrix without forming intermetallic compounds. In this study, the MgLiZn phase appears when the Al/Zn ratio is 1:4 and 2:3, and the $MgLi_2Al$ phase appears when the Al/Zn ratio is 3:2 and 4:1. The formation of MgLiZn phase might be influenced by several concurrent factors including the critical Al/Zn ratio, the interaction of solubility of Al and Zn elements and the solidification cooling rate, which will be our later research content.

4.2 Effect of Al/Zn ratio on mechanical properties

The addition of Al plays an important role in precipitate strengthening and solid solution strengthening of LAZ series alloys, and its main strengthening effect comes from the $MgLi_2Al$ and AlLi phases [27,28]. The solubility of Zn element in LAZ series alloys is high, and solid solution strengthening is its main strengthening mechanism. In this study, the LAZ814 and LAZ823 alloys have higher Zn content to form supersaturated solid solution and the remaining Zn forms the MgLiZn phase, while the LAZ832 and LAZ841 alloys have lower Zn content and limited solid solution strengthening effect. No Zn-containing intermetallic compound is detected in the LAZ832 and LAZ841 alloys, but the precipitate strengthening of Al plays a major strengthening role in the four as-cast LAZ alloys. The UTS of the LAZ alloy increases as the Al content increases.

It can be seen from Fig. 9(b) that after the solid solution treatment at 300 °C for 4 h, the increasing extent of UTS increases with the increase of Zn content, and the UTS of the LAZ814 reaches 271.9 MPa and increases by 42.8%, compared with that of as-cast alloy, which is the largest increasing extent among the four LAZ alloys. It is mainly because the MgLiZn phase in the LAZ814 alloy decomposes and the solid solution strengthening

effect is greatly enhanced. It can be seen from Figs. 5(a) and 7(a) that the precipitates after solid solution are greatly reduced. While only a small amount of $MgLi_2Al$ and AlLi phases in the LAZ832 and LAZ841 alloys decompose to solid solution strengthening, and the increasing extent of strength is small. It can be deduced that the decomposition of MgLiZn particles is the main factor for the improvement of mechanical properties.

After solid solution treatment at 350 °C for 4 h, the AlLi phase decomposes. There is tiny AlLi phase in the LAZ814 and LAZ823 alloys and the microstructure does not change significantly, so their strength does not change obviously. However, a large amount of AlLi phase in the LAZ832 and LAZ841 alloys decomposes, their strength is obviously improved, and the microstructure of α-Mg in the LAZ832 alloy changes from dendritic to smooth, so its UTS increases the most compared to that of the alloy after solid solution treatment at 300 °C for 4 h, increasing by 26.8% to 315.0 MPa. Therefore, it can be inferred that the decomposition of Al−Li phases is the main factor for the improvement of tensile properties of the LAZ alloys.

Figure 13(a) shows the UTS of the four LAZ alloys under different states, and Figs. 13(b, c) show the YS and UTS models obtained by fitting the tensile data of the four LAZ alloys, respectively. Based on these models, the mechanical properties of the alloys at different solid solution temperatures can be roughly estimated.

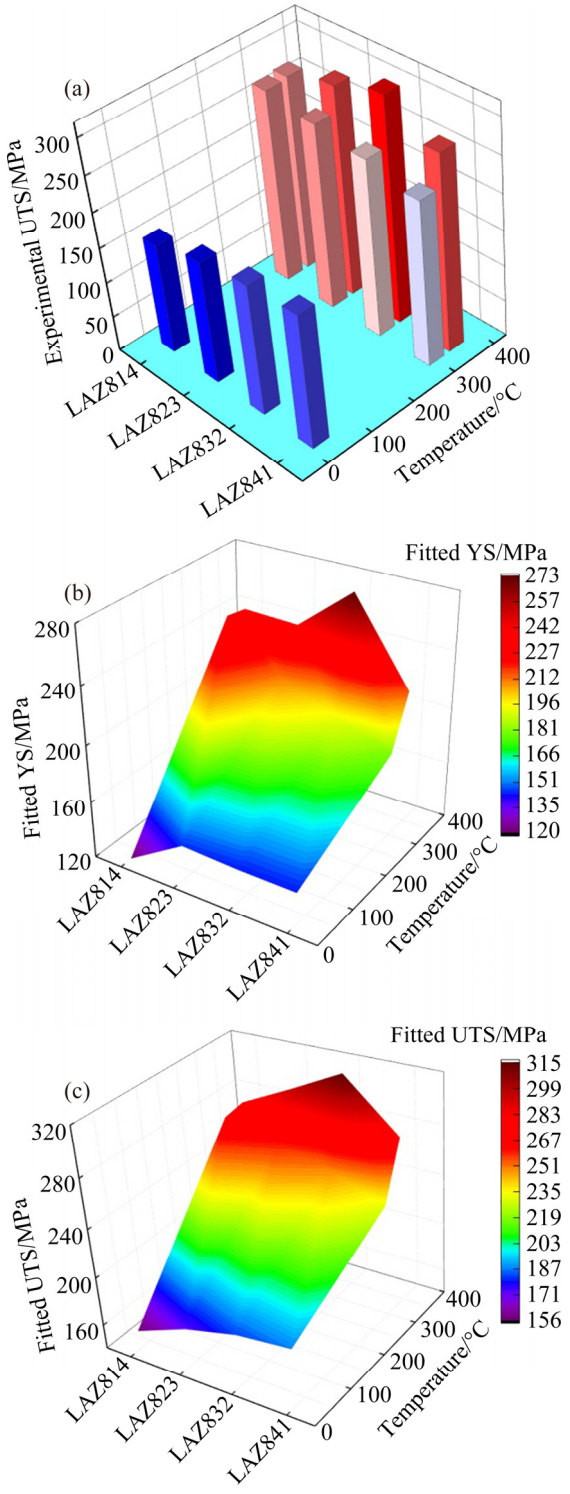

Fig. 13 Mechanical properties visual diagrams of LAZ alloys: (a) 3D histogram model of UTS; (b) Fitted YS; (c) Fitted UTS

5 Conclusions

(1) In the as-cast Mg−8Li−xAl−yZn (x+y=5) alloys, when the Al/Zn ratio is 1:4 and 2:3, the second phases in the stuidied LAZ alloys are mainly AlLi and MgLiZn phases; when the Al/Zn ratios are 3:2 and 4:1, the second phases in the stuidied LAZ alloys are mainly AlLi and $MgLi_2Al$ phases. With the increase of Al content, the UTS of the as-cast LAZ alloys increases and the EL decreases. The strengthening effect of Al is higher than that of Zn element.

(2) The secondary phases partially dissolve after solid solution treatment. The analysis shows that the decomposition temperature of MgLiZn phase is about 300 °C, while the decomposition temperatures of AlLi and $MgLi_2Al$ phases are higher (~350 °C). The solid solution strengthening of Al and Zn elements is found to be the main strengthening way in the solid solution treated LAZ alloys at different temperatures of 300 and 350 °C.

(3) In the as-cast and solid solution treated Mg−8Li−*x*Al−*y*Zn (*x*+*y*=5) alloys, the Mg−8Li−3Al−2Zn alloy after solution treatment at 350 °C for 4 h has the best comprehensive properties (YS=272.5 MPa, UTS=315.0 MPa and EL=3.4%).

Acknowledgments

The authors are grateful for the financial supports from the National Natural Science Foundation of China (51771115, 51775334), Joint Fund for Space Science and Technology (6141B06310106), China and National Defense Science and Technology Innovation Special Zone Project (002-002-01), China.

References

[1] TANG Yan, JIA Wei-tao, LIU Xuan, LE Qi-chi, CUI Jian-zhong. Precipitation evolution during annealing of Mg−Li alloys [J]. Materials Science and Engineering A, 2017, 689: 9−16.

[2] SUN Yue-hua, WANG Ri-chu, PENG Chao-qun, FENG Yan, YANG Ming. Recent progress in Mg−Li matrix composites [J]. Transactions of Nonferrous Metals Society of China, 2019, 29: 1−14.

[3] ZOU Yun, ZHANG Le-hao, LI Yang, WANG Hong-tao, LIU Jia-bin, LIAW P K, BEI Hong-bin, ZHANG Zhong-wu. Improvement of mechanical behaviors of a superlight Mg−Li base alloy by duplex phases and fine precipitates [J]. Journal of Alloys and Compounds, 2018, 735: 2625−2633.

[4] WU Rui-zhi, MURR L E, ZHANG Mi-lin. Recent progress in magnesium−lithium alloys [J]. International Materials Reviews, 2014, 60: 65−100.

[5] CHANG Li-li, SHI Chun-chang, CUI Hong-wei. Enhancement of mechanical properties of duplex Mg−9Li−3Al alloy by Sn and Y addition [J]. Transactions of Nonferrous Metals Society of China, 2018, 28: 30−35.

[6] ZHANG Yang, ZHANG Jie, WU Guo-hua, LIU Wen-cai, ZHANG Liang, DING Wen-jiang. Microstructure and tensile properties of as-extruded Mg−Li−Zn−Gd alloys reforced with icosahedral quasicrystal phase [J]. Materials & Design, 2015, 66: 162−168.

[7] FENG Shi, ZHAO Jiong, LIU Wen-cai, WU Guo-hua, ZHANG Hao-hao, DING Wen-jiang. Effect of extrusion ratio on microstructure and mechanical properties of Mg−8Li−3Al−2Zn−0.5Y alloy with duplex structure [J]. Materials Science and Engineering A, 2017, 692: 9−16.

[8] FAN Cai-he, ZHENG Dong-sheng, CHEN Xi-hong, YANG Jian-jun, LIU Yong, LI Hui-zhong. Effect of large strain cross rolling on microstructure and properties of Al−Li alloy plates with high magnesium content [J]. Transactions of Nonferrous Metals Society of China, 2019, 29: 263−269.

[9] ZHANG Cai-lin, HAN Pei-de, ZHANG Zhu-xia, DONG Ming-hui, ZHANG Li-li, GU Xiang-yang, YANG Yan-qing, XU Bing-she. Transformation of the *θ*-phase in Mg−Li−Al alloys: A density functional theory study [J]. Journal of Molecular Modeling, 2012, 18: 1123−1127.

[10] YANG Yan, XIONG Xiao-ming, SU Jun-fei, PENG Xiao-dong, WEN Hai-ming, WEI Guo-bing, PAN Fu-sheng, LAVERNIA E J. Influence of extrusion temperature on microstructure and mechanical behavior of duplex Mg−Li−Al−Sr alloy [J]. Journal of Alloys and Compounds, 2018, 750: 696−705.

[11] LIN Hai-yi, WU Rui-zhi, FEI Peng-fei, LENG Zhe, GUO Xu-ying, ZHANG Jing-huai, LIU Bin, ZHANG Mi-lin. The solution and aging behavior of Mg−8Li−3Al−*x*Ce(*x*=0, 1.0) alloys [J]. Metallic Materials, 2016, 52: 47−55.

[12] OROVCIK L, RANACHOWAKI Z, SVEC P, KUDELA S Jr, BAJANA O. Strengthening in dual-phase structured Mg−Li−Zn alloys [J]. Kovove Materialy, 2016, 54: 483−489.

[13] KUDELA S Jr, SVEC P, BAJANA O, OROVCIK L, RANACHOWSKI Z. Saffil alumina fibers reinforced dual-phase Mg−Li and Mg−Li−Zn alloys [J]. Kovove Materialy, 2017, 55: 195−203.

[14] JI Hao, LIU Wen-cai, WU Guo-hua, OUYANG Si-jie, GAO Zhan-kui, PENG Xiang, DING Wen-jiang. Influence of Er addition on microstructure and mechanical properties of as-cast Mg−10Li−5Zn alloy [J]. Materials Science and Engineering A, 2019, 739: 395−403.

[15] ZHAO Jiong, LI Zhong-quan, LIU Wen-cai, ZHANG Jie, TIAN Ying, WU Guo-hua. Influence of heat treatment on microstructure and mechanical properties of as-cast Mg−8Li−3Al−2Zn−*x*Y alloy with duplex structure [J]. Materials Science and Engineering A, 2016, 669: 87−94.

[16] ZHOU Yu-cheng, CHEN Zhao-yun, JI Jing-han, SUN Zhi-jie. Effects of second phases on deformation behavior and dynamic recrystallization of as-cast Mg−4.3Li−4.1Zn−1.4Y alloy during hot compression [J]. Journal of Alloys and Compounds, 2019, 770: 540−548.

[17] CAO Fu-rong, ZHOU Bi-jin, DING Xin, ZHANG Jian, XU Guan-ming. Mechanical properties and microstructural evolution in a superlight Mg−7.28Li−2.19Al−0.091Y alloy fabricated by rolling [J]. Journal of Alloys and Compounds, 2018, 745: 436−445.

[18] WU Rui-zhi, ZHANG Mi-lin. Microstructure, mechanical properties and aging behavior of Mg−5Li−3Al−2Zn−*x*Ag [J]. Materials Science and Engineering A, 2009, 520: 36−39.

[19] YANG Chung-wei. Effect of friction stir processing on the microstructural evolution and tensile behaviors of an *α*/*β* dual-phase Mg−Li−Al−Zn alloy [J]. Materials Transactions, 2014, 55: 371−377.

[20] JI Hao, ZHANG Xiao-long, LIU Wen-cai, WU Guo-hua, ZHANG Liang, DING Wen-jiang. Balance of mechanical properties of Mg−8Li−3Al−2Zn−0.5Y alloy by solution and low-temperature aging treatment [J]. Journal of Alloys and Compounds, 2019, 791: 655−664.

[21] SHIN I, CARTER E A. First-principles simulations of plasticity in body-centered cubic magnesium−lithium alloys [J]. Acta Materialia, 2014, 64: 198−207.

[22] LENTZ M, KLAUS M, BEYERLEIN I J, ZECEVIC M, REIMERS W, KNEZEVIC M. In situ X-ray diffraction and crystal plasticity modeling of the deformation behavior of extruded Mg−Li−(Al) alloys: An uncommon tension−compression asymmetry [J]. Acta Materialia, 2015, 86: 254−268.

[23] GUO Xu-ying, WU Rui-zhi, ZHANG Jing-huai, LIU Bin, ZHANG Min-lin. Influences of solid solution parameters on the microstructure and hardness of Mg−9Li−6Al and Mg−9Li−6Al−2Y [J]. Materials & Design, 2014, 53: 528−533.

[24] OUYANG Si-jie, LIU Wen-cai, WU Guo-hua, JI Hao, GAO Zhan-kui, PENG Xiang, LI Zhong-quna, DING Wen-jiang. Microstructure and mechanical properties of as-cast Mg−8Li−*x*Zn−*y*Gd (*x*=1, 2, 3, 4; *y*=1, 2) alloys [J]. Transactions of Nonferrous Metals Society of China, 2019, 29: 1211−1222.

[25] WU Horng-yu, LIN Jia-yu, GAO Zhen-wei, CHEN Hung-wei. Effects of age heat treatment and thermomechanical processing on microstructure and mechanical behavior of LAZ1010 Mg alloy [J]. Materials Science and Engineering A, 2009, 523: 7−12.

[26] ZHONG Hao, PENG Lin-ping, LIU Pei-ying, ZHOU Tie-tao. Design of a Mg−Li−Al−Zn alloy by means of CALPHAD approach [J]. Journal of Computer-aided Materials Design, 2004, 10: 191−199.

[27] PUGAZHENDHI B S, KAR A, SINNAERUVADI K, SUWAS S. Effect of aluminum on microstructure, mechanical property and texture evolution of dual phase Mg−8Li alloy in different processing conditions [J]. Archives of Civil and Mechanical Engineering, 2018, 18: 1332−1344.

[28] KIM J T, JEONG H J, MOON Y, KIM K B, SON H T, JEON C, SIM J W. Microstructure and mechanical properties of the as-cast and warm rolled Mg−9Li−*x*(Al−Si)−*y*Ti alloys with *x*=1, 3, 5 and *y*=0.05 wt.% [J]. Journal of Alloys and Compounds, 2017, 711: 243−249.

铸态和固溶态 Mg−8Li−*x*Al−*y*Zn 合金的显微组织与力学性能

梁新理[1]，彭 翔[1]，冀 浩[1]，刘文才[1]，吴国华[1,2]，丁文江[1,2]

1. 上海交通大学 材料科学与工程学院 轻合金精密成型国家工程研究中心，上海 200240；
2. 上海交通大学 材料科学与工程学院 金属基复合材料国家重点实验室，上海 200240

摘 要：研究 Al/Zn 比(质量比)对 Mg−8Li 合金显微组织和力学性能的影响。结果发现，对于铸态 Mg−8Li−*x*Al−*y*Zn(*x*+*y*=5)合金，当 Al/Zn 比分别为 1:4 和 2:3 时，合金中的第二相主要为 AlLi 和 MgLiZn 相；而当 Al/Zn 比分别为 3:2 和 4:1 时，合金中的第二相主要为 AlLi 和 $MgLi_2Al$ 相。MgLiZn 相的分解温度约为 300 °C，AlLi 和 $MgLi_2Al$ 相的分解温度较高，约为 350 °C。固溶强化是提高 Mg−8Li−*x*Al−*y*Zn 合金强度的主要因素，Mg−8Li−3Al−2Zn 合金在 350 °C 固溶处理 4 h 后具有最佳的综合力学性能，其屈服强度、抗拉强度和伸长率分别为 272.5 MPa、315.0 MPa 和 3.4%。

关键词：镁锂合金；Al/Zn 比；显微组织；力学性能

(Edited by Wei-ping CHEN)